A&A 486, 131–142 (2008)
DOI: 10.1051/0004-6361:20079297

Astronomy & Astrophysics

The Hα Galaxy Survey*

VI. Star-forming companions of nearby field galaxies

P. A. James[1], J. O'Neill[2], and N. S. Shane[1,3]

[1] Astrophysics Research Institute, Liverpool John Moores University, Twelve Quays House, Egerton Wharf, Birkenhead CH41 1LD, UK
e-mail: paj@astro.livjm.ac.uk
[2] Wirral Grammar School for Girls, Heath Road, Bebington, Wirral CH63 3AF, UK
[3] Planetary Science Group, Mullard Space Science Laboratory, Holmbury St. Mary, Dorking, Surrey RH5 6NT, UK

Received 20 December 2007 / Accepted 5 May 2008

ABSTRACT

Aims. We searched for star-forming satellite galaxies that are close enough to their parent galaxies to be considered analogues of the Magellanic Clouds.
Methods. Our search technique relied on the detection of the satellites in continuum-subtracted narrow-band Hα imaging of the central galaxies, which removes most of the background and foreground line-of-sight companions, thus giving a high probability that we are detecting true satellites. The search was performed for 119 central galaxies at distances between 20 and 40 Mpc, although spatial incompleteness means that we have effectively searched 53 full satellite-containing volumes.
Results. We find only 9 "probable" star-forming satellites, around 9 different central galaxies, and 2 more "possible" satellites. After incompleteness correction, this is equivalent to 0.17/0.21 satellites per central galaxy. This frequency is unchanged whether we consider all central galaxy types or just those of Hubble types S0a–Sc, i.e. only the more luminous and massive spiral types. The satellites found are generally similar to the Magellanic Clouds and to field Sm and Im galaxies, in terms of their normalised star formation rates. However, this conclusion is somewhat circular as the similarity of properties to known Sm/Im galaxies was used as a classification criterion. The Small Magellanic Cloud is just below the median values of both star formation rate and *R*-band luminosity of the 9 probable satellites. The Large Magellanic Cloud, however, has a higher *R*-band luminosity than any of the 9 and is only exceeded in star formation rate by the one satellite that appears to be undergoing a tidally-induced starburst. Thus the Milky Way appears to be quite unusual, both in having two star-forming satellite galaxies and in the high luminosity of the Large Magellanic Cloud.

Key words. galaxies: general – galaxies: spiral – galaxies: irregular – galaxies: stellar content – galaxies: statistics – galaxies: Magellanic Clouds

1. Introduction

Satellite galaxies are of great importance in our understanding of the formation and morphological evolution of all types of galaxy. Minor mergers of disk and dwarf galaxies provide one possible process for forming or enlarging bulges (e.g. Haynes et al. 2000; Kannappan et al. 2004; Eliche-Moral et al. 2006), and the associated tidal perturbation is likely to distort and ultimately thicken disks (Quinn & Goodman 1986; Quinn et al. 1993). Indeed, several minor mergers may suffice to convert a disk galaxy into an elliptical (Bournaud et al. 2007; Kaviraj et al. 2007). Gas-rich dwarfs may provide gas reservoirs for rejuvenating early-type disk galaxies and thus prolonging or re-establishing star formation (SF) activity (White & Frenk 1991; Hau et al. 2008), whilst also changing the metallicity of the remaining gas component. Finally, accretion of dwarf galaxies may be very significant for the formation of the stellar haloes of galaxies (e.g. Searle & Zinn 1978; Read et al. 2006).

However, in order to quantify the typical effects of such mergers on disk galaxies, it is necessary to know what fraction actually have close companions, and how many of these contain significant gas reservoirs. These fractions, when combined with a typical time for the decay of orbits through dynamical friction, should ultimately enable an estimate to be made of the minor merger rate, and the resulting impact on the SF of the central galaxies.

A starting-point for such an investigation is provided by the Milky Way, which has a significant number of satellite galaxies. Of these, most are very faint and low-surface brightness dwarf spheroidal and dwarf irregular galaxies; in terms of mass, and future evolutionary impact, by far the most dominant of the probable satellites are the Large and Small Magellanic Clouds (LMC and SMC henceforth). Since the Milky Way is often assumed to be a typical field galaxy, probably of type SBb–SBc, with a total luminosity close to the characteristic value $L^\star$ in the Schechter (1976) luminosity function, it might be natural to assume that Magellanic Cloud-like companions are also typical of the field galaxy population. Indeed, there are several well-studied bright satellites around local galaxies, such as M 32 and NGC 205, the early-type companions of M 31. However, no systematic search

* Based on observations made with the Jacobus Kapteyn Telescope operated on the island of La Palma by the Isaac Newton Group in the Spanish Observatorio del Roque de los Muchachos of the Instituto de Astrofísica de Canarias.

for Magellanic-type companions around a representative sample of field galaxies has yet been carried out, so it is not clear whether the Milky Way is typical or unusual in having two near neighbours of this type.

Some studies of field galaxy companions have been presented in the literature. Zaritsky et al. (1997) searched for companions at least 2.2 mag fainter than the primary galaxy, within 1000 km s^{-1} in velocity and 500 kpc in projected separation, and found 115 satellites around 69 primary galaxies. However, the allowed separations are very much greater than the separation of the Magellanic Clouds from the Milky Way, and Zaritsky et al. (1997) comment that some of the primaries have four or five companions, and these systems may thus be better regarded as galaxy groups. Only about 10% of the companions have projected separations less than 70 kpc, potentially comparable to the Magellanic Clouds. Noeske et al. (2001) found ∼30% of a sample of field dwarf galaxies to have companions within a projected separation of 100 kpc and a recession velocity difference of ±500 km s^{-1}. Madore et al. (2004), following a pioneering study by Bothun & Sullivan (1977), performed a search for companions around isolated elliptical galaxies. Within a 75 kpc projected radius they found 1.0 ± 0.5 companions per elliptical galaxy, higher than the 0.12 ± 0.42 companions per galaxy found by Bothun & Sullivan (1977).

One requirement of any such study is for recession velocity information to remove line-of-sight pairs, which generally dominate the population of apparent pairs found in pure imaging studies, particularly for blue companions (Chen 2008). A complicating factor in obtaining such data through spectroscopic surveys is the problem of fibre collisions with multi-object spectrographs, which means that close pairs are under-represented in many existing surveys. Here we undertake a search using an alternative method based on narrow-band Hα imaging of the areas around field galaxies in the local Universe. Specifically, we search for star forming companions of these galaxies, which will show up via Hα line emission, and as a result this study says nothing about non-star forming companions. Any companions detected in Hα are likely, given the ∼50 Angstrom width of Hα filters used, to be truly associated with central target galaxy. The velocity range for Hα to lie within the same narrow-band filter is ±1000 km s^{-1}, which excludes projected companions with good efficiency, but the number of detected companions will be an upper limit as there will still be some line-of-sight projections within this range. Thus the radial distance range in which satellites could lie is 29 Mpc in depth for an assumed Hubble constant of 70 km s^{-1} Mpc^{-1}; as explained in Sect. 5, we search for satellites to a projected distance of 75 kpc in the plane of the sky, giving a total search volume of ∼0.5 Mpc^3. Of course, any "true" satellites will lie in a much smaller volume than this about the central galaxy. There is also the possibility of including very distant background galaxies, with other emission lines redshifted into the Hα filter bandpass.

Whilst this technique will clearly detect only the line-emitting fraction of all satellite galaxies, it is important to note recent results demonstrating that this is equivalent to the entire gas-rich population in the equivalent mass range, i.e. that there are no or very few quiescent gas-rich galaxies. Meurer et al. (2006) found that all 93 of the HI-selected galaxies in their sample were detected in Hα emission. Haines et al. (2007), using SDSS data, found all of the ∼600 low-luminosity galaxies studied ($-18 < M_r < -16$) in the lowest-density environments to have Hα emission. The previous paper in this series (James et al. 2008) found that all 117 late-type Sm and Im galaxies in the HαGS sample are actively forming stars, and these correspond to more than 50% of the galaxies of these types satisfying the selection criteria of this sample. Thus possession of significant gas reservoirs and star formation (with corresponding Hα emission) appear to be synonymous.

2. Data and methods

We use imaging data from the Hα Galaxy Survey (James et al. 2004), HαGS henceforth. This survey contains data for 327 galaxies selected from the Uppsala General Catalogue of Galaxies (Nilson 1973) (UGC) to have diameters between 1.′7 and 6.′0, measured recession velocities of less than 3000 km s^{-1}, major-to-minor axis ratios less than 4.0, and Hubble type later than S0a. The Virgo cluster core was excluded, so this is effectively a field galaxy sample, but otherwise it should be unbiased with respect to presence or absence of companion or satellite galaxies.

The HαGS data comprise broad-band *R* imaging, and Hα in one of several narrow band filters, selected to match the recession velocity of the target UGC galaxy, obtained at the 1.0 m Jacobus Kapteyn Telescope. The field of view of the JKT CCD camera was ∼11 × 11 arcmin, but we conservatively use only the central 9.5 × 9.5 arcmin area to avoid vignetting and cosmetic problems with the edges of the frames. The Hα images used here were continuum-subtracted, using either observations in an intermediate-width continuum filter, or scaled *R*-band exposures, and flux calibrated, as outlined in James et al. (2004). All galaxy distances (from Virgo-infall corrected recession velocities) and *R*-band magnitudes for the central galaxies used in the present analysis are those listed in Table 3 of James et al. (2004). However, for consistency with the analysis presented in James et al. (2008) (hereafter referred to as Paper V), the SF rates for central galaxies used here are multiplied by a factor 0.7, consistent with the assumption of a "Salpeter light" stellar initial mass function, rather than the Salpeter function assumed by Kennicutt (1998) and adopted in Paper I.

All HαGS galaxies with distances greater than or equal to 20 Mpc were included in this analysis; this was a total of 119 central galaxies. Galaxies within this distance limit were excluded because of the small effective volume included within the CCD field of view. The method employed when searching for potential satellite galaxies was initially to scan the continuum-subtracted Hα images, looking for any apparent regions of emission that are detached from the main galaxy. Any potential sources found were then "blinked" with the *R*-band image (which is aligned to sub-pixel accuracy) to check for, e.g., poorly-subtracted foreground stars, cosmetic defects or bright cosmic ray trails. The brightest of such spurious sources can be excluded from consideration if they are not present in the *R*-band image (since this filter includes the Hα emission), and they can also be excluded if not at least as extended as the stellar point spread function. In most of the frames studied, the situation was completely unambiguous, as no possible satellite galaxies were seen on the Hα frame, and almost all of the spurious objects were quickly identified as such. This left 32 cases where an apparently real emission-line source was identified somewhere within the CCD field of view.

One possible source of incompleteness concerns those galaxies for which the Hα line from the central galaxy lies close to the edge of the bandpass of the narrow band filter used. There is significant overlap between the redshifted Hα filters that were available for use with the JKT, so this was not a severe problem, but there is a small effect for those galaxies lying close to the "changeover" recession velocity from one

filter to the next. To quantify this, the filter throughputs were calculated for each galaxy recession velocity, and for velocities 300 km s^{-1} on either side of this to represent the kinematic limits of likely satellite populations. The most severe bias found was for UGC 4260, where the galaxy itself lies just on the "wrong" side of a changeover point; adding 300 km s^{-1} to this velocity drops the filter throughput to 62% of the value at the galaxy recession velocity. There are 4 cases where this throughput drop at ±300 km s^{-1} is 69 or 70%, 19 cases from 71 to 75%, and 7 cases from 76 to 80%. For the remaining 88 out of 119 galaxies, the throughput across the entire likely satellite velocity range is greater than 80% of that at the galaxy recession velocity.

The flux limit for our Hα images was calculated from faint sources in real images, including photon noise and systematic effects due to irregularities in the background "sky" regions. A moderately extended source like our putative companions would be detected at 5σ for an observed Hα plus [NII] flux of 4.3×10^{-18} W m^{-2}. This corresponds to a SF rate of 0.004–0.0076 $M_\odot$ yr^{-1} for a galaxy at a distance of 30 Mpc, with the exact value in the range depending on the extinction corrections adopted.

The remaining, and distinctly problematic issue concerning the 32 putative satellites was to distinguish whether these sources were truly separate galaxies, or just outlying SF regions of the central galaxy. Conservatively, all 32 sources were included for further analysis, even where the appearance on the *R*-band image pointed towards the latter being the case, and resolution of this question was left to further analysis of the source properties in Sect. 3 below. This analysis was based on total Hα and *R*-band fluxes of the companions, which were measured using matched elliptical apertures. The Hα fluxes were then converted to SF rates using the conversion formula of Kennicutt (1998) scaled by the 0.7 factor mentioned above, but with internal extinction corrections based on companion object M_R-magnitudes using the methods of Helmboldt et al. (2004).

3. Classification of putative satellite galaxies

The first stage in separating the 32 Hα-emitting sources into true companions and outlying HII regions was to examine their distributions of SF rate and *R*-band luminosity, as shown in Fig. 1. The range of SF rates is broadly consistent with those found in Magellanic dwarf galaxies, but in the *R*-band luminosity distribution there is already the hint of bimodality, with two components around 10^7 and $10^{8.5}$ $L_\odot$. The Magellanic Clouds are included in this plot (crosses), with the SF rates having been calculated from the Hα data of Kennicutt & Hodge (1986), using the same method of correcting for internal extinction as was applied to the SF rates of the putative satellite galaxies. Both Magellanic Clouds lie in the group of higher luminosity objects in Fig. 1.

Figure 2 shows the projected separation of the putative companion from the nucleus of the central galaxy, plotted against the companion *R*-band luminosity in solar units. This figure adds weight to the supposition that the candidate companions with lower luminosities in the *R*-band are HII regions rather than separate galaxies, as they show a strong tendency to lie closer to the central galaxy than do the brighter sources.

A further plot used to discriminate between HII regions and satellite galaxies makes use of the SF timescale, a parameter explored extensively in Paper V. The SF timescale is given by the total stellar mass of the galaxy divided by the current SF rate, such that a constant SF rate throughout a galaxy's history would result in a SF timescale of a Hubble time. As explained in

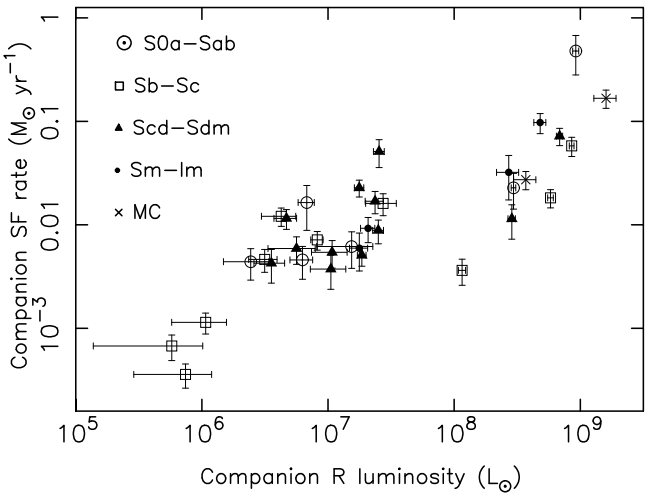

Fig. 1. SF rate vs. *R*-band luminosity for the 32 possible companion galaxies, with the Magellanic Cloud properties shown for comparison (crosses). The different points show the Hubble type of the central UGC galaxy.

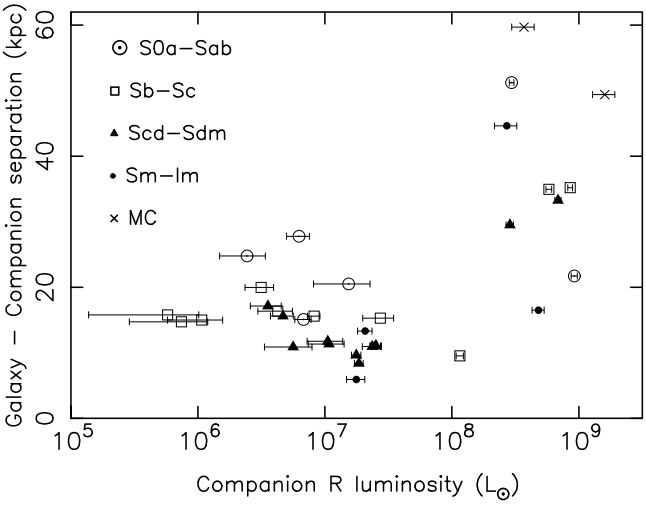

Fig. 2. Separation of the companion object and central galaxy in kpc vs. the *R*-band luminosity of the companion. The separation plotted is the actual distance for the Magellanic Clouds, and the projected separation on the sky for the other objects.

Paper V, the total stellar mass is derived from *R*-band photometry, with an adopted *R*-band mass-to-light ratio for late-type dwarfs of 0.65, based on the models of Bell & de Jong (2001). The timescale is increased by a factor of 1.67 to account for gas recycling of 40% of the mass of any new generation of stars (van Zee 2001).

As was concluded in Paper V, Fig. 3 shows the field Sm and Im late-type galaxies from the HαGS sample to scatter around a mean SF timescale of just under a Hubble time, indicating approximately constant SF activity in these galaxies. The crosses show the positions of the LMC and SMC within this distribution, where the Magellanic Cloud values are based on SF rates from the Hα measurements of Kennicutt & Hodge (1986). Interestingly, both lie close to the centre of the range of SF timescales of the field galaxies, with values of ~10–15 Gyr.

The brightest, and hence highest mass, of the putative satellite galaxies also lie within the distribution of field galaxies shown in Fig. 3, and thus appear similar in their stellar

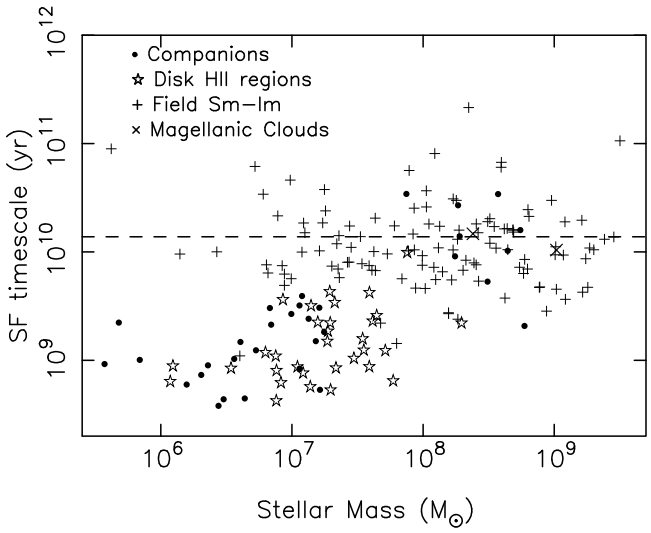

Fig. 3. The time required to form the total stellar mass of the system, for the putative satellite galaxies, the Magellanic Clouds, field Sm and Im galaxies from the HαGS survey, and disk HII regions, vs. stellar mass.

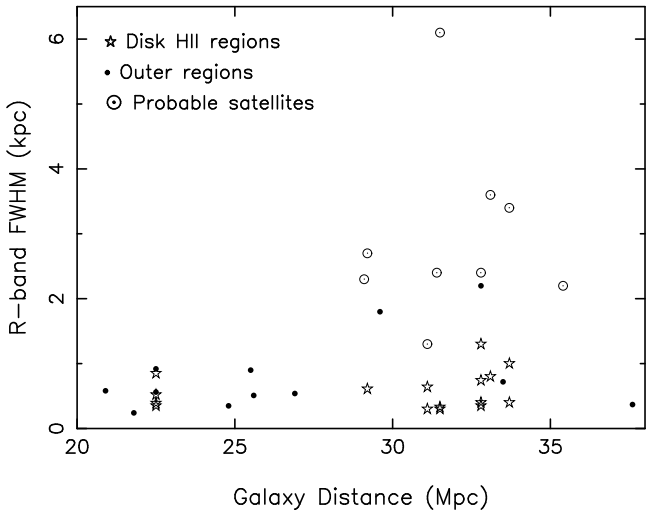

Fig. 4. The *FWHM* sizes in kpc of the 9 satellite galaxies, a selection of disk HII regions, and the outer disk regions, measured from *R*-band images.

masses and current SF activity to field Sm and Im galaxies. The one bright satellite which is displaced somewhat to a short SF timescale is the companion to UGC 4541, which appears tidally disturbed and may be undergoing an interaction-induced starburst or other nuclear activity. However, *all* of the putative companions with stellar masses below $\sim 5 \times 10^7$ $M_\odot$ have short SF timescales of $<10^{10}$ yr, and the average for these objects is $<10^9$ yr. This is most simply explained if these objects are SF regions in the outer disks of the central HαGS galaxies, which would naturally have low SF timescales since they represent short-lived local enhancements in the SF rate of their host galaxies. This is confirmed by the position of known HII regions from the disk regions of HαGS galaxies, shown as stars in Fig. 3. The existence of SF at a low level in the outer regions of disk galaxies has also been noted in UV imaging from the GALEX mission (Thilker et al. 2005; Gil de Paz et al. 2005).

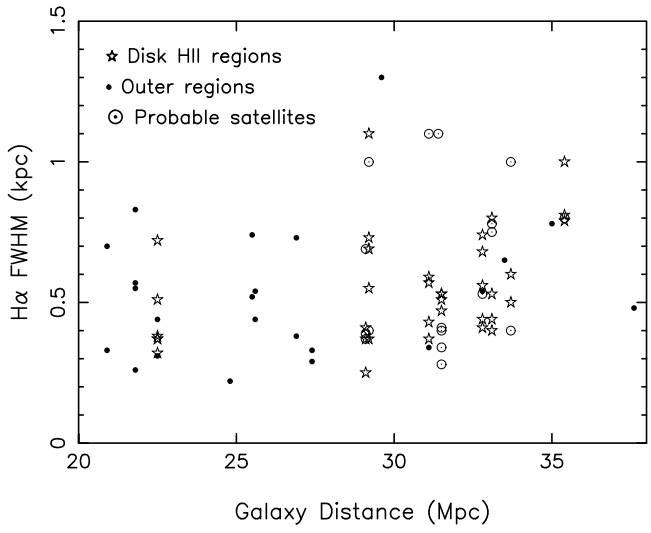

Fig. 5. The *FWHM* sizes in kpc of the Hα emission-line regions detected by SExtractor within the 9 satellite galaxies and the outer disk regions, compared with the equivalent dimension for disk HII regions.

However, even though Figs. 1 and 3 indicate that the 32 objects split into two groups as described in the previous paragraph, they are not completely conclusive. In particular, objects in the high luminosity/mass end of the distribution of probable outer HII regions lie on the outskirts of the distribution of field Sm and Im galaxies in Fig. 3. As a final test, the sizes of the objects were measured from our *R*-band and Hα images, and plotted in Figs. 4 and 5. In both figures, the sizes were determined in a completely automated and objective fashion, using Full Width at Half Maximum (*FWHM*) values from the SExtractor package. The resulting *R*-band sizes are plotted against the distance to the central galaxy in Mpc, in Fig. 4. This confirms that all 9 of the likely satellite galaxies are very extended in terms of their continuum emission, with *FWHM* sizes of 1.5–6.0 kpc. Many of the probable outer disk sources are too faint in the *R*-band to be picked up as separate sources by the SExtractor software; most of the remainder have *R*-band *FWHM* sizes between 0.2 and 1.0 kpc, identical to the range of sizes of disk HII regions, also shown in Fig. 4 for comparison. However, two of the "outer disk" objects do show significant extents in the *R*-band images. These are objects associated with UGC 3530 and UGC 4260, with *R*-band extents of 1.8 and 2.2 kpc respectively. Both objects are amongst the most massive of the 23 "outer disk" objects, at just over 10^7 $M_\odot$, and have star-formation timescales of $\sim$1 and 2.5 Gyr respectively. Thus these may be satellite galaxies in a star-bursting phase, and we will keep them in our analysis as "possible" satellites. Images of these objects are shown in Appendix A, with the putative satellites indicated by lines above and to one side of their location.

The Hα sizes of objects, plotted on the *y*-axis in Fig. 5, show no significant dependence on object type. The SExtractor algorithm split the likely satellite galaxies into separate resolved HII regions in several cases, and the resulting regions had *FWHM* sizes consistent with those of both the 23 outlying regions (all of which were detected in the Hα analysis), and a selection of disk HII regions. The mean *FWHM* of 36 disk HII regions was 0.55 kpc (standard deviation 0.19 kpc, standard error on the mean 0.03 kpc); for the 23 outlying regions, the mean was 0.55 kpc (s.d. 0.24 kpc, s.e. 0.05 kpc); and for the

Table 1. Main properties of the central and satellite galaxies.

UGC_c	$Type_c$	Dist Mpc	SFR_c $M_\odot$ yr^{-1}	δSFR_c	$R_{tot,c}$ mag	$\delta R_{tot,c}$	$L_{R,c}$ $L_\odot$	SFR_s $M_\odot$ yr^{-1}	δSFR_s	$L_{R,s}$ $L_\odot$	$\delta L_{R,s}$	Sepn kpc
2603	Im	33.7	0.28	0.10	14.59	0.06	9.70(08)	0.032	0.015	2.71(8)	5.4(7)	44.6
4273	SBb	35.4	1.92	0.36	11.84	0.04	1.36(10)	0.018	0.004	5.81(8)	3.0(7)	35.0
4362	S0a	33.1	0.46	0.17	11.96	0.04	1.06(10)	0.023	0.009	2.96(8)	1.2(7)	51.2
4469	SBcd	31.5	1.52	0.25	12.50	0.04	5.81(09)	0.072	0.014	6.86(8)	3.9(7)	33.3
4541	Sa	31.4	0.21	0.06	11.37	0.04	1.63(10)	0.478	0.197	9.21(8)	5.0(7)	21.7
4574	SBb	31.1	2.96	0.60	11.26	0.04	1.77(10)	0.058	0.012	8.55(8)	3.7(7)	35.2
5688	SBm	29.2	0.44	0.08	13.57	0.05	1.87(09)	0.097	0.021	4.81(8)	5.2(7)	16.5
6506	SBd	29.1	0.06	0.02	14.74	0.06	6.31(08)	0.011	0.004	2.86(8)	1.9(7)	29.5
12788	Sc	32.8	1.54	0.30	12.51	0.04	6.25(09)	0.004	0.001	1.16(8)	7.6(6)	9.5

9 probable satellites, which were detected as 17 HII regions, the mean *FWHM* was 0.63 kpc (s.d. 0.29 kpc, s.e. 0.07 kpc).

Henceforth, we consider only the 9 companion objects with *R*-band luminosities greater than 10^8 $L_\odot$ to be "probable" satellite galaxies, and the companions to UGC 3530 and UGC 4260 as "possible" satellites. The remaining 21 objects are consistent with being outer disk HII regions in terms of all the parameters considered here. However, they will be targetted for spectroscopic follow-up in future work (outlined in Sect. 7 of this paper).

4. Properties of the 9 probable satellite galaxies

The main data for the 9 probable satellite galaxies are presented in Table 1, which is organised as follows. Columns 1 and 2 give the UGC number and classification of the central galaxy, with the latter being taken from the NASA Extragalactic Database (NED henceforth). Column 3 gives the distance for the system, calculated from the central galaxy recession velocity, using a Virgo-infall corrected model (James et al. 2004). Columns 4 and 5 give the Hα-derived SF rate and error for the central galaxy, and Cols. 6 and 7 the *R*-band total magnitude and error. The corresponding *R*-band luminosity in solar units is given in Col. 8. Columns 9 and 10 give the SF rate and error for the satellite galaxy, calculated as described in Sect. 2, and Cols. 11 and 12 the satellite galaxy *R*-band luminosity and error. The final column lists the projected separation in kpc between the centres of the central and satellite galaxies. This assumes that central and satellite galaxies are at the same distance, as listed in Col. 3.

Images of the 9 galaxy systems are shown in Appendix B. In each case, the upper *R*-band image is a sufficiently wide field to show both central and satellite galaxies, and again lines have been added to indicate the location of the satellites. The satellites are shown in more detail in the lower images, with the *R*-band image on the left and the continuum-subtracted Hα image on the right. In every case, even the upper image shows only a subset of the area searched for satellites.

Our method of identifying companions as likely satellites relies on the detection of line emission in a narrow-band filter selected to include Hα from the central galaxy. This method is not foolproof, and it is possible that some of the putative satellites are background galaxies with shorter-wavelength lines redshifted into the same bandpass. One check for this is to search for previously catalogued recession velocities for the 9 satellites in the literature. The results of this search, using the NED "Search for Objects Near Object Name" facility, are given in Table 2. All bar one had names or identifiers in at least one catalogue or survey, listed in the second column of Table 2; the angular separation between central and satellite galaxies is given in arcmin in Col. 3, and in kpc in Col. 4. Only 3 satellites had separate

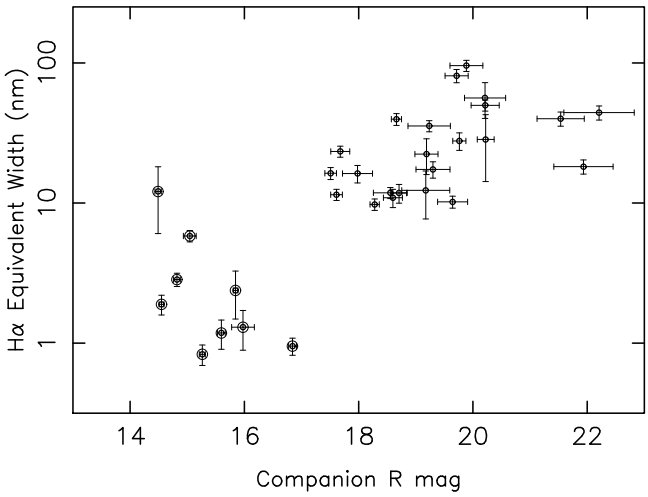

Fig. 6. The Hα equivalent width values for the 9 satellite galaxies and the outer disk regions, plotted against total *R*-band mag.

recession velocities; these are listed in Col. 5, with the central galaxy recession velocities being in the final column. All 3 satellite velocities lie within ~100 km s^{-1} of that of the central galaxy, which gives some confidence in our methods.

Comments on individual galaxies:

UGC 2603 – the main galaxy is classified as an Im, so this can be considered a binary pair rather than a central plus satellite system. The satellite galaxy has substantially higher surface brightness in *R*-band continuum than the HαGS galaxy, but fairly diffuse Hα emission.

UGC 4273 – the companion is one of the most weakly detected in Hα but this has an independent recession velocity listed in NED, which is very close to that of the central galaxy.

UGC 4362 – the companion is bright in the *R*-band image, and shows strong SF with clumpy, resolved HII regions, but has not been previously catalogued according to NED. The companion is on the extreme edge of the CCD frame so the measured SF rate and *R*-band luminosities in Table 1 should be considered as lower limits, although the majority of the companion does appear to have been imaged, from inspection of sky survey images of this field.

UGC 4469 – the companion is clearly a Magellanic irregular, with clumpy Hα emission indicating several off-centre HII regions. There is an independent recession velocity for the companion in NED, again very close to that of the the central galaxy.

UGC 4541 – this system appears to be undergoing significant tidal disturbance; unsurprisingly, the catalogued recession velocity of the companion is close to that of UGC 4541. The Hα

Table 2. Catalogue names and recession properties of previously-identified satellite galaxies.

UGC_c	Satellite name	Separation (arcmin)	Separation (kpc)	V_{rec} sat (km s^{-1})	V_{rec} cent (km s^{-1})
2603	2MASXJ03192345+8116238	4.4	43.1	–	2516
4273	KUG0809+363	3.5	36.0	2483	2471
4362	–	–	–	–	2344
4469	NGC 2406B	3.6	33.0	2104	2078
4541	CGCG 060-036	2.4	21.9	2115	2060
4574	2MASXJ08482381+7402176	3.9	35.3	–	2160
5688	VV 294b	1.9	16.1	–	1920
6506	MAPS-NGP O_319_1199567	3.6	30.5	–	1580
12788	UM 007 NED01	1.0	9.5	–	2956

morphology of the companion reveals a strong nuclear starburst and/or AGN activity; the strength of the Hα emission results in the short SF timescale found for this object in Sect. 3.

UGC 4574 – the Hα image of the companion shows two clumps of SF, located at either end of the moderately elongated *R*-band light distribution.

UGC 5688 – the central galaxy has low *R*-band luminosity and surface brightness. The Hα image shows clumps of emission from both ends of the elongated *R*-band light distribution, like the companion of UGC 4574, resembling the pattern of SF seen in many galaxy bars.

UGC 6506 – this is a similar case to UGC 2603 and UGC 5688, with a low luminosity central galaxy, and this should probably be considered a binary system rather than as a central galaxy with a satellite.

UGC 12788 – the putative companion is projected on the outer disk of the central galaxy, but does not look like an HII region or part of a spiral arm. This is a possible case of tidal interaction, revealed in the distorted and strongly star-forming arm in UGC 12788, close to the putative companion. However, it should be noted that the object considered here to be a companion galaxy is listed in NED as "West HII region in UGC 12788".

Two of the central/satellite systems studied by Zaritsky et al. (1997) are in the current sample. The first is NGC 5921 and and its companion, identified by Zaritsky et al. (1997) as NGC 5921: [ZSF97]b. This companion is clearly detected in our data, both in *R*-band and Hα emission, and indeed was independently selected as a putative satellite (it is the square at SF rate = 0.012 $M_\odot$ yr^{-1}, *R*-band luminosity 4×10^6 $L_\odot$ in Fig. 1). However, this region, along with one other similar region in NGC 5921 (not identified by Zaritsky et al. 1997), was considered highly likely to be an outer HII region. The second of the systems listed by Zaritsky et al. (1997) is NGC 5962 and the companion they identify as NGC 5962: [ZSF97]b. The region containing the latter was searched in the present study, but the companion is present only as a very faint *R*-band source, with no detected Hα emission.

The NED "Search for Objects Near Object Name" was also carried out for the 23 outer disk objects. None of these was found to have a measured recession velocity, and the only two to have individual NED entries are both classified as HII regions, one in UGC 9935/NGC 5964 (Bradley et al. 2006), and one in UGC 12343/NGC 7479 (Rozas et al. 1999).

5. Statistics of star forming satellites

The next stage of the analysis is to look at the numbers of star-forming satellites found, to put constraints on the overall abundance of such systems around field galaxies. Given that the regions around 119 HαGS galaxies were searched, 9 satellites found seems a small number, given that we have two such systems around the Milky Way, but in order to make this comparison quantitative we need to correct for sources of incompleteness in our search method.

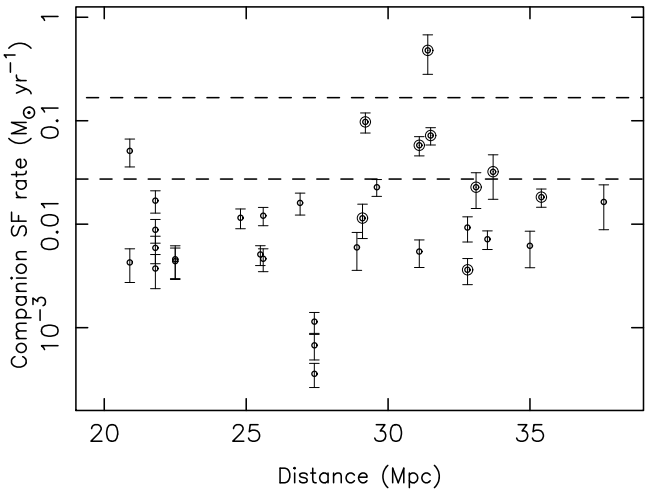

Fig. 7. Companion object SF rate vs. the distance of the central object, in Mpc. The dashed lines show the SF rates corresponding to the LMC (upper line) and SMC (lower line), demonstrating that we can detect companions with SF rates much lower than those of the Magellanic Clouds to the limits of our survey. The ringed points indicate the 9 probable satellite galaxies, as explained in Sect. 3.

As a starting point for this analysis, we need to confirm that our data and methods are sufficiently sensitive to detect "Magellanic Cloud like" satellites. Figure 7 shows the Hα-derived SF rates for 32 regions identified in the current paper as possible satellites, with the ringed points identifying the 9 likely satellites. These rates are plotted against the distance in Mpc of the central galaxy in the system, and the horizontal lines show the SF rates of the Magellanic Clouds. This confirms that our Hα technique is easily sensitive enough to detect star forming galaxies fainter than the Magellanic Clouds to the spatial limits of our survey, as objects with Hα luminosities significantly lower than that of the SMC are seen over the full range of distances studied.

Surface brightness is also important in determining the detectability of galaxies; it is possible that Magellanic-type companions with quite high total SF rates could be missed if the line emission were very extended and hence of low surface brightness. This possibility is investigated in Fig. 8, which is similar to Fig. 7, but with the SF rate of each region divided by its area in kpc^2, measured from our Hα images. The same quantity for the Magellanic Clouds is again shown by the dashed

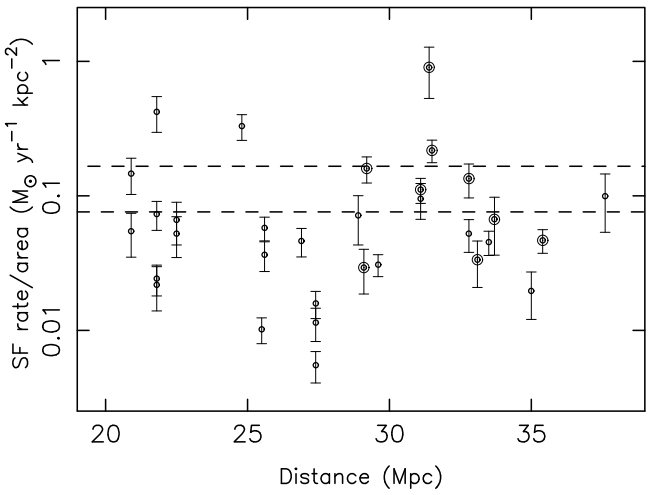

Fig. 8. Companion object SF rate per unit area vs. the distance of the central object, in Mpc. The dashed lines show the SF rates per unit area corresponding to the LMC (upper line) and SMC (lower line), demonstrating that we can detect companions with SF surface densities much lower than those of the Magellanic Clouds to the limits of our survey. The ringed points indicate the 9 probable satellite galaxies, as explained in Sect. 3.

lines. The latter values were derived from Kennicutt & Hodge (1986), who give Hα flux measurements measured in large apertures comparable in kpc sizes to the apertures used to measure the Hα fluxes in our companion objects. Specifically, Kennicutt & Hodge (1986) find 25% of the Hα flux from the LMC to come from a 30 arcmin aperture centred on 30 Doradus; this would be both spatially resolved at the distance of our satellite galaxies, and easily detectable in surface brightness as shown from the position of the upper dashed line in Fig. 8. Similarly, the lower dashed line comes from a 16 arcmin aperture flux measurement on the SMC, which contains 17% of the total Hα emission and hence of the inferred SF activity in that galaxy. Thus we can again conclude that Magellanic-type galaxies should be easily detectable with our data and techniques.

In order to calculate incompleteness corrections, it is necessary to decide on a definition of a close companion galaxy. For the present work, a "Magellanic-type" companion is defined to be one that lies within a spherical region, centred on the UGC galaxy, with a volume twice as large as the volume that just contains both the Magellanic Clouds. This corresponds to a radial separation of less than $60 \times \sqrt[3]{2} = 75.2$ kpc, where 60 kpc is our adopted distance to the SMC. However, for any given galaxy, it is not possible to see the full volume potentially occupied by satellites. For closer galaxies, the outlying parts of the volume are missed as they lie outside the CCD field of view. In addition, there is a "blank spot" along the line-of-sight of the main galaxy, in all cases, as the Hα emission from any companion would be confused with that of the central galaxy, in our narrow-band images. Knowing the distance of each of the central galaxies, their optical major and minor axes, and the size of the imaged field, it is then possible to calculate the fraction of the spherical halo volume that is missed due to these two causes. This fraction was then assumed to be equal to the fraction of satellites that were missed, i.e. implicitly assuming that satellites were equally likely to be found anywhere within the spherical volume. In support of this assumption, several studies have found satellite distributions to be isotropic, for blue central galaxies such as those studied here (Yang et al. 2006; Agustsson & Brainerd 2007; Azzaro et al. 2007).

Table 3. The number of central galaxies studied, broken down by Hubble type, and the frequency with which they host star-forming satellites.

T-type	$N_{\rm Gal}$	$N_{\rm Corr}$	$N_{\rm Sat}$	$N_{\rm Sat}/N_{\rm Corr}$
0	6	2.4	1	$0.42^{+0.97}_{-0.35}$
1	7	3.5	1	$0.29^{+0.67}_{-0.24}$
2	4	2.1	0	$0.00^{+0.88}_{-0.00}$
3	15	7.2	2	$0.28^{+0.37}_{-0.18}$
4	15	6.8	0	$0.00^{+0.27}_{-0.00}$
5	14	5.9	1	$0.17^{+0.39}_{-0.14}$
6	15	6.5	1	$0.15^{+0.35}_{-0.12}$
7	14	5.7	1	$0.18^{+0.41}_{-0.15}$
8	13	5.5	0	$0.00^{+0.33}_{-0.00}$
9	6	2.4	1	$0.42^{+0.97}_{-0.35}$
10	10	4.6	1	$0.22^{+0.51}_{-0.18}$
0–5	61	28.0	5	$0.18^{+0.12}_{-0.08}$
0–10	119	52.7	9	$0.17^{+0.08}_{-0.06}$

A programme was written to calculate the completeness fraction for all 119 of the HαGS galaxies, and the results are summarised in Table 3. This lists, as a function of Hubble T-type, the total numbers of galaxies observed (Col. 2); the sums of the observable fractions of the satellite volumes (Col. 3); the number of star-forming satellites found (Col. 4); and ratio of satellites found to observable volumes, i.e. Col. 4 divided by Col. 3 (listed in the final column). To summarise these results, the 119 potentially satellite-containing volumes were covered with a mean efficiency of just below 50%, resulting in an effective search of 53 volumes. This search yielded 9 star-forming satellites, or $0.17^{+0.08}_{-0.06}$ satellite galaxies per full volume searched. This fraction applies whether all T-types included, or just the more luminous galaxies with T types in the range 0 to 5 (bottom and penultimate lines of Table 3).

The errors quoted here and in the final column of Table 3 are 1-σ limits derived from the tables of Gehrels (1986).

It could be argued that the companion to UGC 12788, which lies inside the projected disk of UGC 12788 but is detected due to its distinctive morphology, should be excluded from these statistics. It should also be noted that some of the detected satellites may actually lie outside the 75.2 kpc radius circle due to projection uncertainties. Thus the fractions listed in the final column of Table 3 could be considered as upper limits for the numbers of "Magellanic Cloud type" companions as we have defined them here. However, we should also take into account to possibility that some of the objects classified as outlying HII regions may in fact be satellite galaxies. If the two "possible" objects identified from their R-band sizes in Fig. 4 are included, the overall fraction of satellites per central galaxy search increases from 0.17 to $0.21^{+0.08}_{-0.06}$. If we very conservatively include all the outlying objects not positively identified elsewhere as being HII regions, the total number increases to 30, for an overall fraction of satellites per galaxy searched of $0.57^{+0.12}_{-0.10}$.

6. Correlation of satellite and central galaxy properties

The search carried out in the present study has identified 9 probable satellite galaxies, with significant stellar masses, in close proximity (in projection) to their central galaxies. Given these properties, it is interesting to check whether the SF activity,

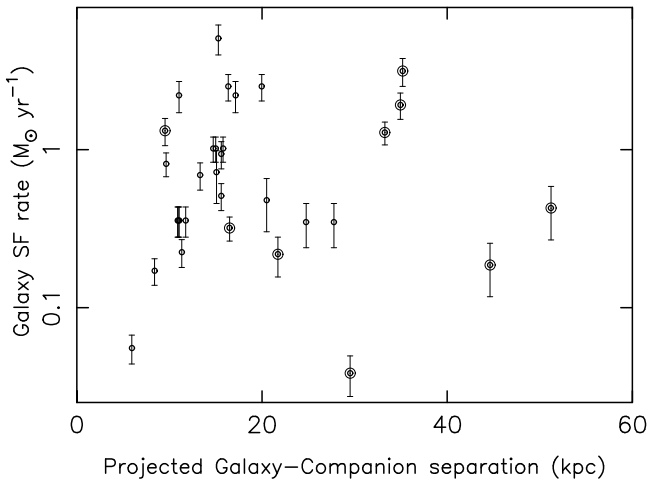

Fig. 9. The central galaxy SF rate plotted against the projected separation of the companion object and the central galaxy. The ringed points indicate the 9 probable satellite galaxies, as explained in Sect. 3.

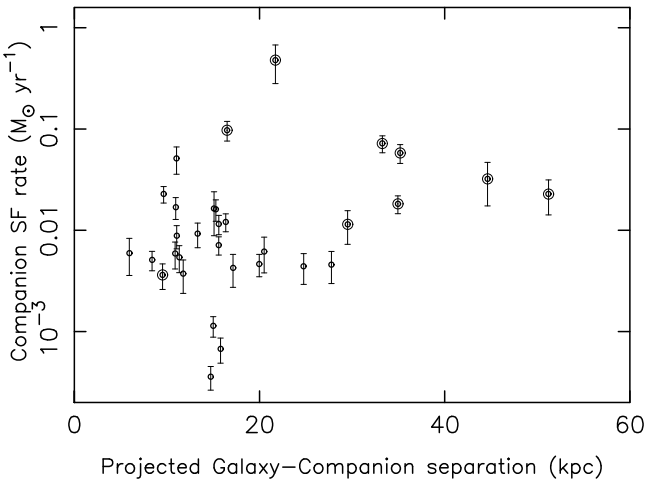

Fig. 10. The SF rate for each companion object plotted against the projected separation of the companion and the central galaxy. The ringed points indicate the 9 probable satellite galaxies, as explained in Sect. 3.

either of the central galaxies or of the probable companions, is affected by the tidal forces between central and satellite galaxies. The overall question of the effect of environment on SF rates for the entire HαGS sample is the subject of a future paper, so this analysis concerns only the subsample of galaxies with identified companions.

Figure 9 shows the Hα-derived SF rates of the central galaxies plotted against projected galaxy-companion separation in kpc. The ringed points indicate the 9 probable satellite systems as identified in Sect. 3. This figure shows no correlation between central galaxy SF rate and projected separation, so there is no obvious effect of the presence of the satellites on their central galaxies. Similarly, Fig. 10 shows no correlation between satellite galaxy SF rate and projected distance from the central galaxy, at least for the 9 probable satellites. There is a significant difference between these probable satellites and the objects identified in Sect. 3 as outlying HII regions, but this is as expected under our preferred interpretation of these objects.

Finally, Fig. 11 shows companion object SF timescales, as defined in Sect. 3, against projected separation between central and satellite galaxies. Again, the only clear result from this plot is the short SF timescales of the outlying HII regions, already identified in Fig. 3. For the 9 probable satellites, no correlation is found between SF timescale and projected separation from their central galaxies. The satellite galaxy with the shortest SF timescale is the companion to UGC 4541; this not the closest galaxy-satellite pair investigated here, but there does appear to be tidal distortion associated with this interaction. The closest pairing in projected separation is UGC 12788 and its companion; here the companion appears completely unaffected by tidal effects, in terms of both optical morphology and SF properties, so it is possible that there is a significant line-of-sight separation in this case. The second closest in apparent separation are UGC 5688 and companion; the latter has a SF timescale below 10 Gyr, which may show a modest enhancement in SF rate as a the result of tidal effects. However, UGC 5688 is a low luminosity galaxy of type SBm, and so tidal effects are likely to be minimal due to the low mass of the primary galaxy.

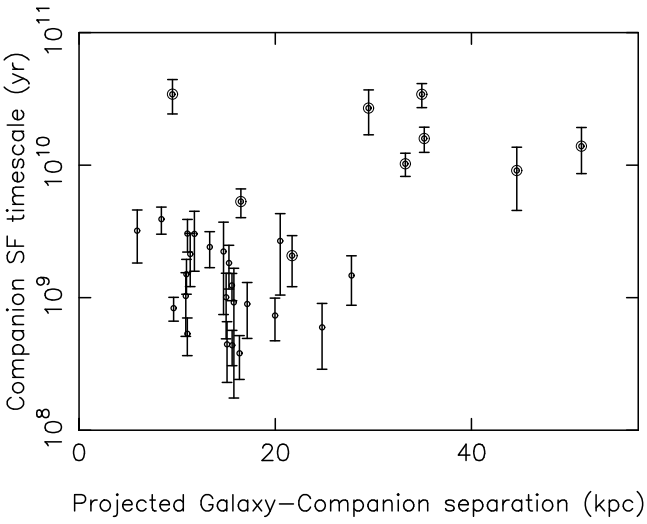

Fig. 11. The SF timescale of each companion object plotted against the projected separation of the companion and the central galaxy. The ringed points indicate the 9 probable satellite galaxies, as explained in Sect. 3.

7. Discussion and future work

The major result of this paper is that actively star-forming satellite galaxies, with luminosities and SF rates within approximately an order of magnitude of those of the Magellanic Clouds, are fairly rare. Most galaxies in our survey of field spirals have no such satellites. Previous searches for satellites of all types (Zaritsky et al. 1997; Madore et al. 2004) have found significantly more than this, typically one substantial satellite per central galaxy surveyed, although it is very difficult to make quantitative comparisons because of the varying depths and methods of the different surveys. However, it does appear likely that most satellites, even of isolated field galaxies, are of non-star forming types. Examples close to home are M 32 and NGC 205, early type companions of the Andromeda spiral M 31. Given that most isolated galaxies of Magellanic-Cloud like luminosities are actively forming stars (Paper V), this would seem to imply the efficient truncation of star formation in satellites, with a timescale short compared to a Hubble time. This then raises

interesting questions about the fate of the gas originally in the satellite dwarfs; is it consumed in a burst of star formation triggered by interaction with the central galaxy, or is a significant fraction of it expelled from the satellite, enabling it to be accreted onto the central galaxy? Evidence of this process in the Milky Way system may be provided by the Magellanic Stream. Given the importance of gas supply in disk galaxy evolution, it would clearly be useful to know the frequency of such gas-yielding interactions, and the timescales and gas masses involved.

Observationally, there are 3 main requirements: to extend the sample size of star-forming satellite candidates; to discriminate definitively between true satellites and outlying parts of disks; and to determine the red-to-blue satellite fraction. The first can simply be done by further Hα imaging, preferably going rather deeper and over wider fields than the present data set. The second requires spectroscopy to determine velocity differences between central and putative satellite galaxies, and preferably velocity cubes (e.g. from Hα Fabry-Perot instruments or HI maps) to look for signs of interaction. Data enabling the identification of quiescent red-sequence satellites are problematic given the greater difficulty of measuring recession velocities for faint and possibly low-surface-brightness absorption line sources, but the situation is being improved with surveys using sensitive multi-fibre instruments. We are actively pursuing all of these approaches.

One caveat on the current results concerns the conclusion that the 9 satellites are fairly similar to the Magellanic Clouds. This can be seen as unsurprising given that we used the similarity to the Magellanic Clouds, particularly in Figs. 1 and 3, to argue for the 9 objects being true satellites. There is indeed circularity in this argument, and it is clearly important to include the provisionally rejected objects in follow-up spectroscopy. Given that the latter tend to be found at small projected separations from the central galaxies and have similar properties to HII regions in Fig. 3, it is likely that this interpretation will be confirmed for most or all of them, but there may be some important objects lurking in this category.

8. Conclusions

This study has identified 9 probable star-forming satellite galaxies with projected separations consistent with their being as close to their central galaxies as the Magellanic Clouds are to the Milky Way. Figure 1 illustrates that the stellar luminosities and SF rates of the Magellanic Clouds are comparable to those of the 9 probable satellites found here. Overall, the satellite galaxies (including the Magellanic Clouds) are currently forming stars at a rate comparable to field Sm and Im galaxies in the HαGS sample. The only evidence of a strong starburst is in the tidally-disturbed companion to UGC 4541. Considering the 9 probable satellites and the Magellanic Clouds together, the LMC and SMC are the brightest and 7th brightest in R-band luminosity, and the 2nd and 9th most rapidly star-forming. Thus the LMC is clearly a large satellite, whereas the SMC is close to or just below average amongst those found here. We find no cases of 2 satellites around any of the 119 central galaxies studied, so the Milky Way appears well-favoured in the number of large star-forming companions in its immediate neighbourhood. In this context, it is interesting to note that Puech et al. (2007) have recently concluded that the MW is distinctive for its *lack* of merging activity over its history; the results found here indicate that any such deficiency is likely to be rectified in the future.

Acknowledgements. The Jacobus Kapteyn Telescope was operated on the island of La Palma by the Isaac Newton Group in the Spanish Observatorio del Roque de los Muchachos of the Instituto de Astrofisica de Canarias. This research has made extensive use of the NASA/IPAC Extragalactic Database (NED) which is operated by the Jet Propulsion Laboratory, California Institute of Technology, under contract with the National Aeronautics and Space Administration. Jane O'Neill contributed to this work while on a summer placement supported by the Nuffield Science Bursary Scheme. PAJ thanks Chris Moss and Sue Percival for useful comments, and the referee is also thanked for many constructive suggestions.

References

Agustsson, I., & Brainerd, T. G. 2007, ArXiv e-prints, 704
Azzaro, M., Patiri, S. G., Prada, F., & Zentner, A. R. 2007, MNRAS, 376, L43
Bell, E. F., & de Jong, R. S. 2001, ApJ, 550, 212
Bothun, G. D., & Sullivan, III, W. T. 1977, PASP, 89, 5
Bournaud, F., Jog, C. J., & Combes, F. 2007, A&A, 476, 1179
Bradley, T. R., Knapen, J. H., Beckman, J. E., & Folkes, S. L. 2006, A&A, 459, L13
Chen, J. 2008, A&A, 484, 347
Eliche-Moral, M. C., Balcells, M., Aguerri, J. A. L., & González-García, A. C. 2006, A&A, 457, 91
Gehrels, N. 1986, ApJ, 303, 336
Gil de Paz, A., Madore, B. F., Boissier, S., et al. 2005, ApJ, 627, L29
Haines, C. P., Gargiulo, A., La Barbera, F., et al. 2007, MNRAS, 381, 7
Hau, G., Bower, R., Kilborn, V., et al. 2008, MNRAS, 385, 1965
Haynes, M. P., Jore, K. P., Barrett, E. A., Broeils, A. H., & Murray, B. M. 2000, AJ, 120, 703
Helmboldt, J. F., Walterbos, R. A. M., Bothun, G. D., O'Neil, K., & de Blok, W. J. G. 2004, ApJ, 613, 914
James, P. A., Shane, N. S., Beckman, J. E., et al. 2004, A&A, 414, 23
James, P. A., Prescott, M., & Baldry, I. K. 2008, ArXiv e-prints, 804
Kannappan, S. J., Jansen, R. A., & Barton, E. J. 2004, AJ, 127, 1371
Kaviraj, S., Peirani, S., Khochfar, S., Silk, J., & Kay, S. 2007, ArXiv e-prints, 711
Kennicutt, R. C. 1998, ARA&A, 36, 189
Kennicutt, Jr., R. C., & Hodge, P. W. 1986, ApJ, 306, 130
Madore, B. F., Freedman, W. L., & Bothun, G. D. 2004, ApJ, 607, 810
Meurer, G. R., Hanish, D. J., Ferguson, H. C., et al. 2006, ApJS, 165, 307
Nilson, P. 1973, Uppsala general catalogue of galaxies (Acta Universitatis Upsaliensis. Nova Acta Regiae Societatis Scientiarum Upsaliensis – Uppsala Astronomiska Observatoriums Annaler, Uppsala: Astronomiska Observatorium, 1973)
Noeske, K. G., Iglesias-Páramo, J., Vílchez, J. M., Papaderos, P., & Fricke, K. J. 2001, A&A, 371, 806
Puech, M., Hammer, F., Chemin, L., Flores, H., & Lehnert, M. 2007, ArXiv e-prints, 711
Quinn, P. J., & Goodman, J. 1986, ApJ, 309, 472
Quinn, P. J., Hernquist, L., & Fullagar, D. P. 1993, ApJ, 403, 74
Read, J. I., Pontzen, A. P., & Viel, M. 2006, MNRAS, 371, 885
Rozas, M., Zurita, A., Heller, C. H., & Beckman, J. E. 1999, A&AS, 135, 145
Schechter, P. 1976, ApJ, 203, 297
Searle, L., & Zinn, R. 1978, ApJ, 225, 357
Thilker, D. A., Bianchi, L., Boissier, S., et al. 2005, ApJ, 619, L79
van Zee, L. 2001, AJ, 121, 2003
White, S. D. M., & Frenk, C. S. 1991, ApJ, 379, 52
Yang, X., van den Bosch, F. C., Mo, H. J., et al. 2006, MNRAS, 369, 1293
Zaritsky, D., Smith, R., Frenk, C., & White, S. D. M. 1997, ApJ, 478, 39

Appendix A: Images of the 2 possible satellites and their central galaxies

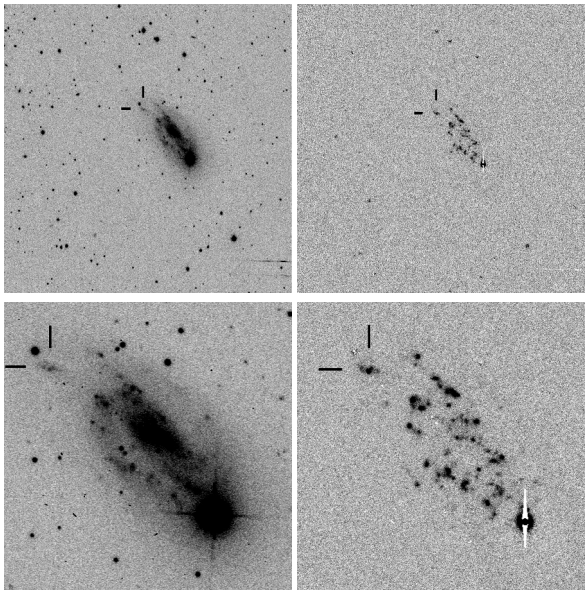

Fig. A.1. Upper images: UGC 3530 and satellite galaxy, showing the full field of view (image size 560″ by 560″); *R*-band (*left*) and Hα (*right*). Lower image: UGC 3530 and satellite galaxy, close-up view (image size 160″ by 160″); *R*-band (*left*) and Hα (*right*).

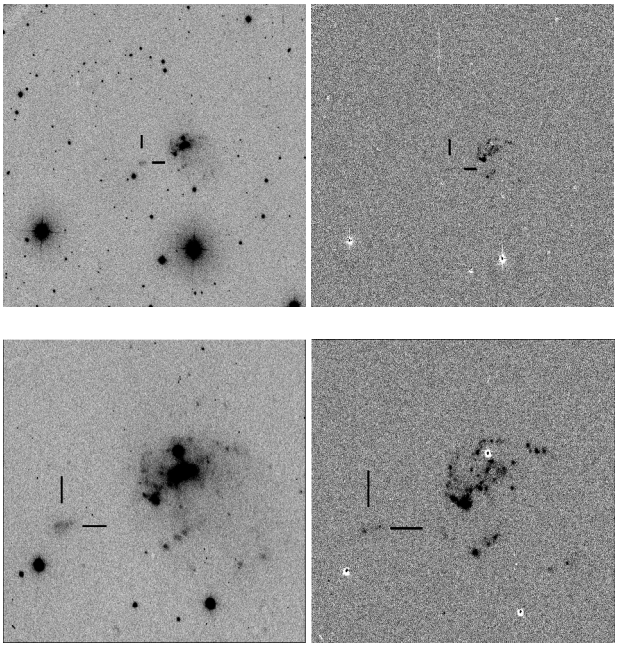

Fig. A.2. Upper images: UGC 4260 and satellite galaxy, showing the full field of view (image size 560″ by 560″); *R*-band (*left*) and Hα (*right*). Lower images: UGC 4260 and satellite galaxy, close-up view (image size 154″ by 154″); *R*-band (*left*) and Hα (*right*).

Appendix B: Images of the 9 probable satellites and their central galaxies

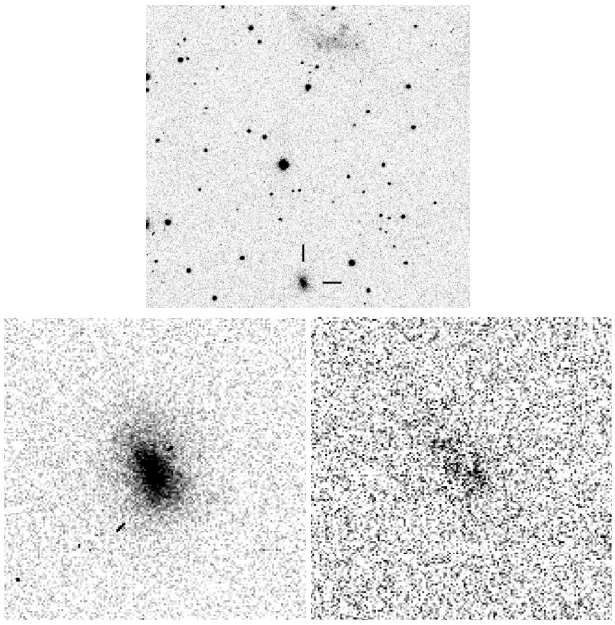

Fig. B.1. Upper image: UGC 2603 and satellite galaxy (image size 343″ by 325″). Lower images: Satellite galaxy in *R*-band (*left*) and continuum-subtracted Hα *right*: image sizes 47″ by 47″).

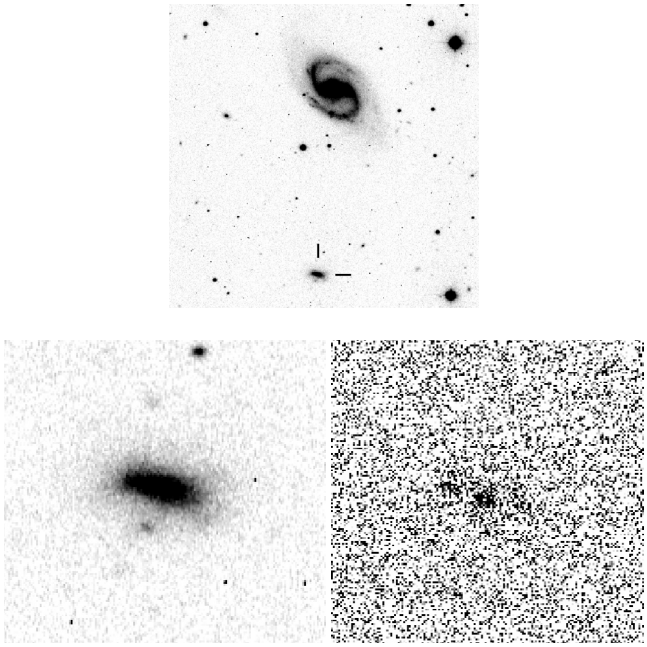

Fig. B.2. Upper image: UGC 4273 and satellite galaxy (image size 338″ by 335″). Lower images: Satellite galaxy in *R*-band (*left*) and continuum-subtracted Hα (*right*: image sizes 56″ by 56″).

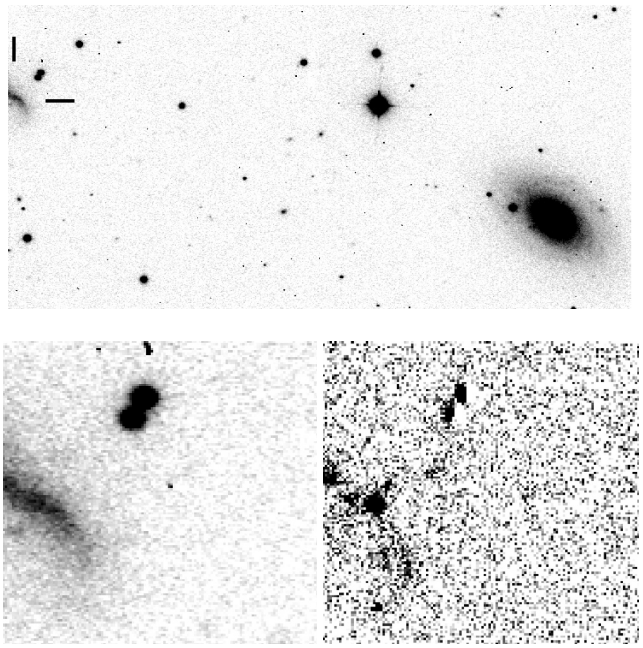

Fig. B.3. Upper image: UGC 4362 and satellite galaxy (image size 359″ by 177″). Lower images: Satellite galaxy in *R*-band (left) and continuum-subtracted Hα (*right*: image sizes 44″ by 44″).

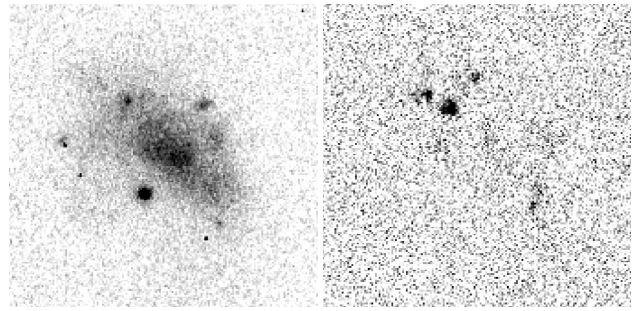

Fig. B.4. Upper image: UGC 4469 and satellite galaxy (image size 248″ by 220″). Lower images: Satellite galaxy in *R*-band (*left*) and continuum-subtracted Hα (*right*: image sizes 51″ by 51″).

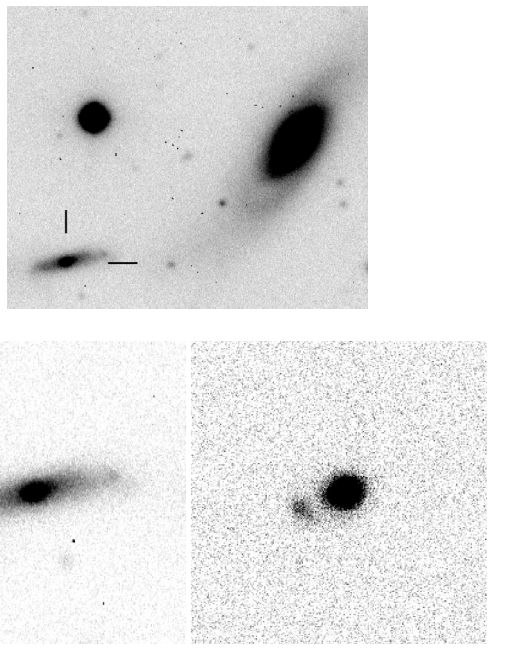

Fig. B.5. Upper image: UGC 4541 and satellite galaxy (image size 196″ by 161″). Lower images: Satellite galaxy in *R*-band (*left*) and continuum-subtracted Hα (*right*: image sizes 78″ by 78″).

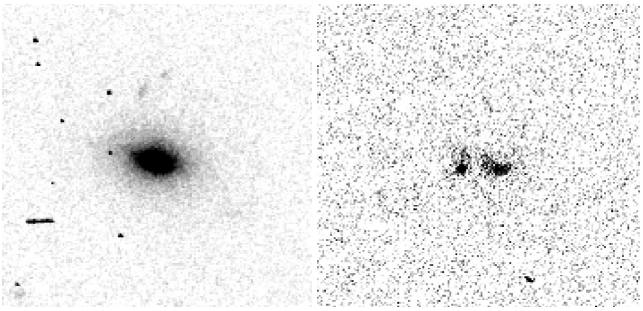

Fig. B.6. Upper image: UGC 4574 and satellite galaxy (image size 318″ by 309″). Lower images: Satellite galaxy in *R*-band (*left*) and continuum-subtracted Hα (*right*: image sizes 53″ by 53″).

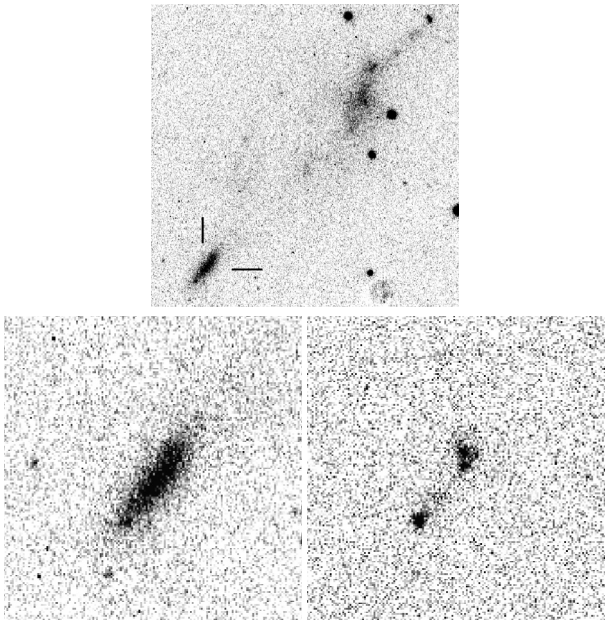

Fig. B.7. Upper image: UGC 5688 and satellite galaxy (image size 160″ by 154″). Lower images: Satellite galaxy in *R*-band (*left*) and continuum-subtracted Hα (*right*: image sizes 51″ by 51″).

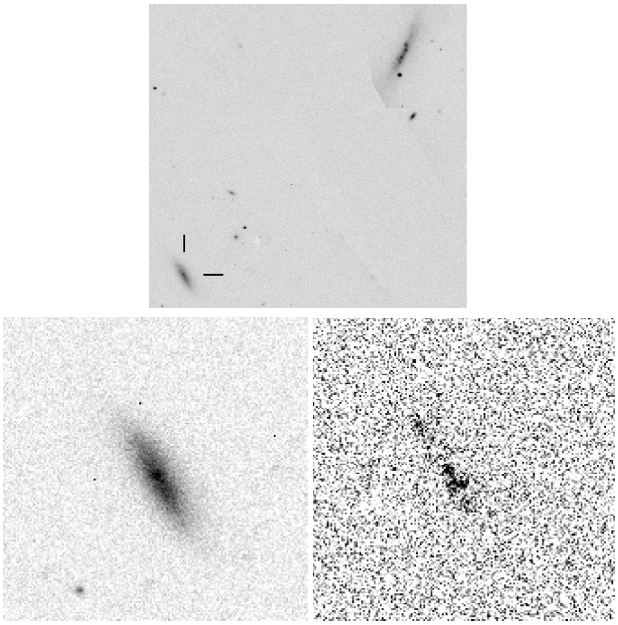

Fig. B.8. Upper image: UGC 6506 and satellite galaxy (image size 212″ by 206″). The central part of this image suffered contamination from a band of scattered light in a diagonal strip between the two galaxies; this has been removed in the data reduction, along with some stars which lie in the centre of this field. The relative brightness and orientation of the two galaxies are not affected. Lower images: Satellite galaxy in *R*-band (*left*) and continuum-subtracted Hα (*right*: image sizes 54″ by 54″).

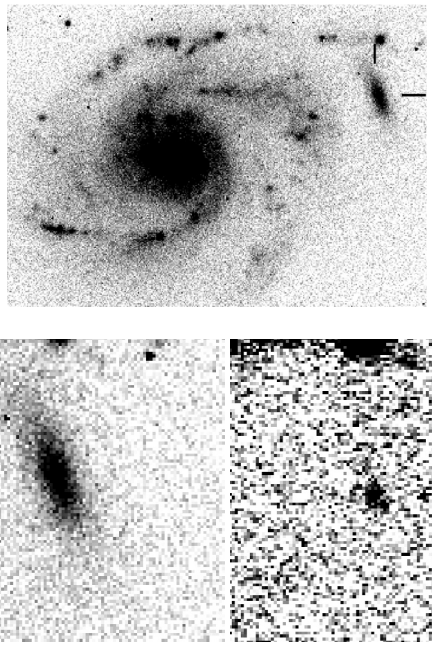

Fig. B.9. Upper image: UGC 12788 and satellite galaxy (image size 113″ by 82″). Lower images: Satellite galaxy in *R*-band (*left*) and continuum-subtracted Hα (*right*: image sizes 33″ by 33″).